Solid State Ionics xxx (2010) xxx–xxx

Contents lists available at ScienceDirect

Solid State Ionics

journal homepage: www.elsevier.com/locate/ssi

CFD modeling of a biogas fuelled SOFC

E. Vakouftsi [a], G.E. Marnellos [a,b,*], C. Athanasiou [b,c], F. Coutelieris [d]

[a] Department of Mechanical Engineering, University of Western Macedonia, Bakola & Sialvera, GR-50100 Kozani, Greece
[b] Chemical Process Engineering Research Institute, Centre for Research & Technology Hellas, 6th km. Charilaou-Thermi Rd., P.O. Box 361, GR-57001 Thermi, Thessaloniki, Greece
[c] Department of Environmental Engineering, Democritus University of Thrace, Bas. Sofias 12, GR-67100 Xanthi, Greece
[d] Department of Environmental and Natural Resources Management, University of Ioannina, G. Seferi 2, GR-30100 Agrinio, Greece

ARTICLE INFO

Available online xxxx

Keywords:
SOFC
Biogas
3D simulation
CFD

ABSTRACT

Mathematical modeling of transport and electrochemical phenomena within SOFCs can lead to improved understanding of the involved physical, electrical, and chemical processes and represents a powerful tool for their development. In this context, the present work illustrates a three-dimensional CFD simulation of a planar SOFC unit cell fuelled by modeled biogas/steam mixtures. The simulations estimate the distribution of gas species, the current densities and the potentials, as well as the temperature gradients and confirm that equimolar CH_4/CO_2 biogas leads to improved performance, while minimal steam addition can prevent carbon deposition.

1. Introduction

Biogas is a renewable fuel containing 50–80%v CH_4 diluted by 50–20%v CO_2 reforming agent. Only 10% of the readily exploitable biogas resources are estimated to be used today due to the local nature of biogas production, which implies the use of internal combustion engines of small nominal power and of low electrical conversion. Moreover, landfill biogas (almost 80% of current biogas production) usually contains less than 50% CH_4, hindering its use in conventional power systems. On the contrary, fuel cells exhibit appreciable electric efficiencies even at high power outputs and diluted fuel [1,2]. Especially, Solid Oxide Fuel Cells (SOFCs) can be directly fed with CH_4/H_2O mixtures and overcome the need to pre-reform biogas or to eliminate CO through successive catalytic reactors [3,4]. Internal steam reforming is the dominant route for SOFCs commercialization [5], while only few preliminary studies, mostly triggered by the prospects of direct biogas SOFC applications, had examined internal dry reforming [6–9].

In parallel to experimental research, SOFC modeling efforts have been intensified during the past decade, leading to a variety of models ranging from the simulation of individual SOFC components (micro-scale) up to the simulation of entire stacks (macro-scale), and vary in complexity and in the nature of the employed assumptions. In this direction, zero-, one-, two-, and three-dimensional models have been developed, mostly based on empirical data, while a number of models describe the electrochemically active region and the electrochemical reactions associated losses [10–15]. The current state-of-art in SOFC modeling refers to the use of computational fluid dynamics (CFD) to result in full-field solutions and to couple them with electrochemical models [16–18]. Due to advantages of internal steam reforming of CH_4, significant research has been dedicated to its simulation [16,17,19,20], while some efforts focus on CH_4 dry reforming [1,2,21], considering detailed flow field, current distribution, $CH_4/H_2O/CO_2/H_2/CO$ transport and heat generation/consumption by chemical and electrochemical reactions and ohmic effects. Especially, the CFD-Ace$^+$ software was used to investigate the minimization of steam addition [22], to address solutions that prevent carbon deposition [23], to identify ohmic losses at the cylindrical geometry [24], and to propose innovative designs for advanced SOFC performance [25].

In the present effort, CFD-Ace$^+$ is used for the 3D simulation of species and temperature distribution, during the internal reforming of various biogas compositions at the inlet region of a planar unit-cell configuration, and to predict the performance, the location of increased thermal stresses and the possibility of solid carbon deposition.

2. Model description

The two dimensional cuts of the examined unit cell (the three-dimensional volume of which was discretized by a structured grid of 33,516 cells) are depicted in Fig. 1. The Ni-YSZ anode and the $La_{0.7}Sr_{0.3}MnO_{3-\alpha}$-YSZ cathode were considered as porous gas diffusion electrodes. In this configuration, a range of biogas/steam mixtures of constant molar flowrate ($2.9\cdot10^{-6}$ mol/s) were fed to the anode compartment in parallel (co-flow) to a cathodic air flowrate ($4.0\cdot10^{-5}$ mol/s), adequate to ensure a slight variation of the oxygen content, throughout the unit volume. The unit cell was assumed to operate at atmospheric pressure (the pressure drop along the anodic and the cathodic flow channels, was calculated to be less than 0.58 and

* Corresponding author. Department of Mechanical Engineering, University of Western Macedonia, Bakola & Sialvera, GR-50100 Kozani, Greece. Tel.: +30 2461 0 56690; fax: +30 2461 0 56601.
E-mail address: gmarnellos@uowm.gr (G.E. Marnellos).

0167-2738/$ – see front matter © 2010 Elsevier B.V. All rights reserved.
doi:10.1016/j.ssi.2010.05.051

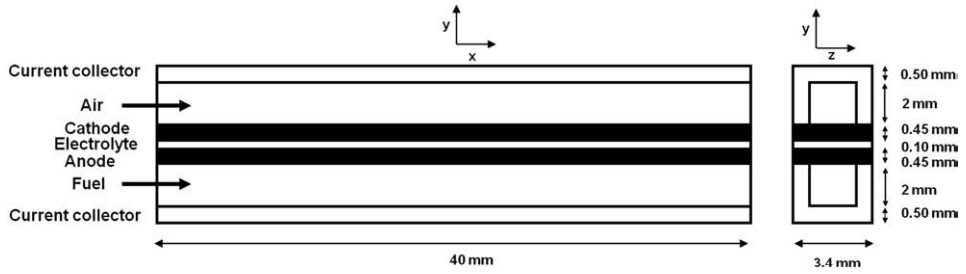

Fig. 1. Simulated geometry of the unit cell (planar configuration).

5.45 Pa, in all cases and varied insignificantly with the examined fuel mixtures). The preheated at 1073 K biogas/steam mixtures were fed to the anode and internally reformed through the linearly independent reactions of steam reforming and water gas shift (WGS):

$$CH_4 + H_2O \leftrightarrow CO + 3H_2 \quad (1)$$

$$CO + H_2O \leftrightarrow CO_2 + H_2 \quad (2)$$

the first assumed to occur at the surface of the Ni catalyst, with a reaction rate expressed in the Arrhenius form [26]:

$$R_1 = 1.91\,10^8 T^2 e^{-27063/T} P_{CH4} P_{H2O} - 1.1\,10^{-7} T^4 e^{-232/T} P_{H2}^3 P_{CO}\ \text{kmol/m}^2\text{s} \quad (3)$$

while the WGS was assumed to take place wherever gas is present, and its homogeneous rate was calculated by the expression [27]:

$$R_{WGS} = 1199 T^2 e^{-12500/T} P_{CO} P_{H2O} - 1119 T^2 e^{-12500/T} P_{CO2} P_{H2}\ \text{kmol/m}^3\text{s}. \quad (4)$$

The kinetics of the anodic electro-oxidation of both H_2 and CO [25]:

$$H_2 + CO + 2O^{2-} \rightarrow H_2O + CO_2 + 4e^- \quad (5)$$

at the triple phase boundary between Ni, YSZ and the gas phase and the cathodic oxygen reduction were described by the Butler–Volmer equation:

$$j_T = \frac{j_0}{\prod_{i=1}^{N}\left[C_{i,ref}\right]^{a_{ie}}}\left[\exp\left(\frac{a_a F}{RT}\eta\right) - \exp\left(\frac{-a_a F}{RT}\eta\right)\right]\prod_{i=1}^{N}[C_i]^{a_{ie}} \quad (6)$$

where $j_o^{anodic} = 10^{11}\ Am^{-3}$ and $j_o^{cathodic} = 10^{10}\ Am^{-3}$ are the exchange current densities for the anodic electrochemical reaction (Eq. (5)) and the cathodic oxygen electro-reduction, respectively, multiplied by the S/V ratio (electrode surface to electrode apparent volume ratio) [22], $\alpha_a = \alpha_c = 0.7$ are the anodic and cathodic charge transfer coefficients [22], $[C_i/C_{i,ref}]$ are the near-wall molar concentrations (mol/m^3) of the electrochemically reactive species (determined numerically by the mass conservation and chemical/electrochemical reaction kinetic equations) [24,28], $a_{ie} = 1$ are the concentration exponents [22], T is the absolute temperature and F, R are the Faraday and the ideal gas constants respectively. The overpotential η was determined locally, within the porous electrode. A constant value of zero potential was set to the anode collector, while the potential of the cathodic collector was set to several discrete values.

The present study presents a mathematical model where flow, mass transport, heat transfer and ion exchange are coupled, while the relative mass, charge, momentum and energy balances (including transport in porous media and the kinetics of the involved chemical/electrochemical reactions) were taken into account [29]. This model has been integrated through three-dimensional simulations for the geometry presented in Fig. 1. Numerical solutions were obtained by the commercial CFD-Ace$^+$ software based on the finite volume method with tolerance of four orders of magnitude (10^{-4}) for all calculated quantities. The assumptions involved laminar flow for compressible fluids, no gravitational effects, Darcy's law for porous regions, no energy transfer by radiation and zero accumulation and mass flux by the walls. The properties of the used materials are listed in Table 1 [25,26].

3. Results and discussion

Two sets of biogas/steam mixtures were examined, the first referring to different biogas compositions ($CH_4/CO_2 = 30/10$, 30/20 and 30/30%v the rest supplemented by steam) within the typical range of biogas CH_4/CO_2 molar ratios (80/20–50/50%v), and for constant methane (this set also included the $CH_4/H_2O = 30/70$%v composition for comparison with internal steam reforming). The second set refers to the equimolar biogas composition ($CH_4/CO_2 = 50/50$%v) for different biogas/steam ratios (90/10, 80/20 and 70/30%v).

3.1. Species distribution

Fig. 2 depicts the variation of $CH_4/CO_2/H_2O$ (a and c) and H_2/CO (b and d) molar fractions, at the interface of the anodic electrode and the gas phase ($y = 2.50$ mm, according to Fig. 1) and the central vertical plane of the anodic chamber ($z = 1.70$ mm), for the aforementioned sets of compositions (a and b for constant CH_4 supply, and c and d for equimolar biogas mixtures). For constant CH_4 (Fig. 2a), its consumption is not affected by the gradual substitution of H_2O by the CO_2 reforming agent, and it is completed in the first two centimeters from the unit cell's inlet, for the given molar flowrate. This can be attributed to the rapid equilibrium of the $CH_4/CO_2/H_2O/H_2/CO$ mixture due to Reactions 1 and 2. On the other hand, the increase of CH_4 content (for equimolar biogas compositions — Fig. 2c), slightly expands the CH_4 consumption region. In all cases (Fig. 2a and c), steam initially decreases, reflecting its role as a reactant for CH_4 reforming, and, within the first centimeter from the unit cell's inlet, increases, as hydrogen is electro-oxidized. For high CO_2 contents (mostly for equimolar biogas), CO_2 behavior is almost the same. Fig. 2c shows that the higher the CO_2 content of the feed, the lower its concentration becomes in the examined four centimeters from the cell's inlet,

Table 1
Properties of the involved materials.

	ε	κ	k_S	A/V	d_p	σ_F	σ_s
		m^2	$Wm^{-1}\,K^{-1}$	m^{-1}	10^{-6} m	$\Omega^{-1}\,m^{-1}$	$10^2\Omega^{-1}\,m^{-1}$
Ni/YSZ	0.40	10^{-12}	6.2	$3\cdot10^6$	1	10	1000
LSM/YSZ	0.50	10^{-12}	9.6	–	1	10	77
YSZ	0.01	10^{-18}	2.7	–	1	10	–

Please cite this article as: E. Vakouftsi, et al., Solid State Ion. (2010), doi:10.1016/j.ssi.2010.05.051

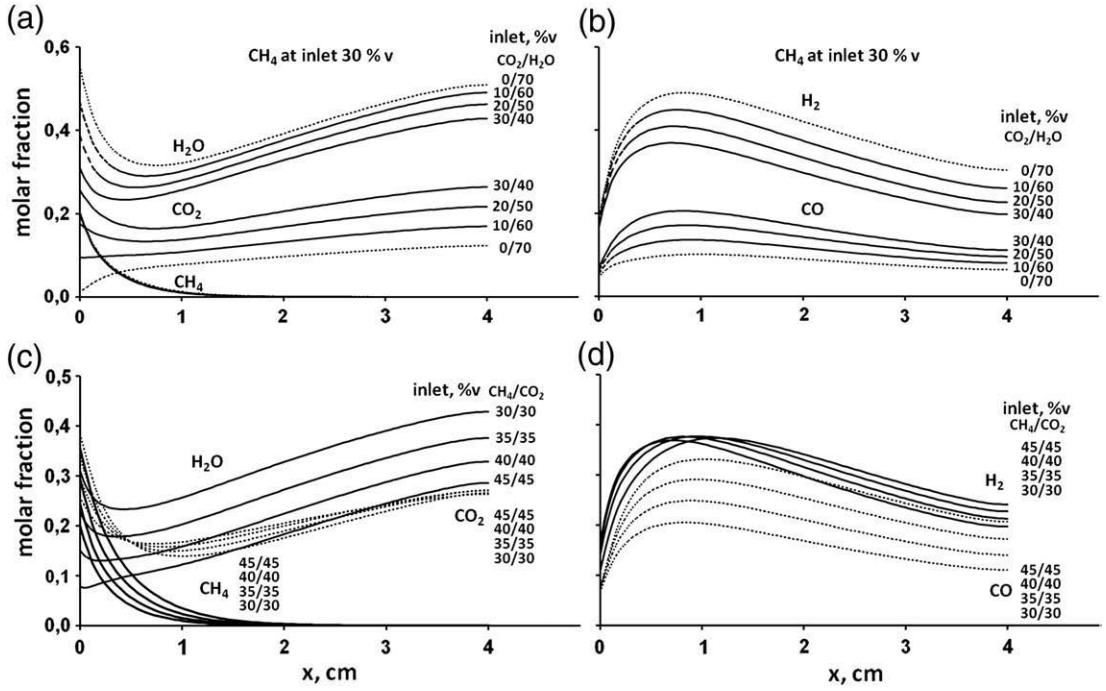

Fig. 2. Chemical species distribution along the anode/gas phase (y = 2.50 mm) central line (z = 0.00 mm) for the examined biogas/steam mixtures (for constant CH_4 inlet: (a) for reactants, (b) for products, and for equimolar $CH_4/CO_2 = 1$ ratio: (c) for reactants, (d) for products), and for an imposed $V_{cell} = 0.5$ V.

although CO electro-oxidation forces the CO_2 lines to coincide beyond this region. The initial decrease of CO_2 denotes the rapid kinetics of the reverse WGS, in the corresponding region, followed by a gradual increase, which can be attributed to rightward shift of Reaction 2 (due to the increase of CO and steam) and the electro-oxidation of CO.

Regarding H_2, its concentration, throughout the cell's inlet region (all four centimeters examined) increases with steam, in case of constant CH_4 (Fig. 2b), and its profile with distance x exhibits a rapid initial rise, in the first half centimeter from the inlet, followed by a gradual drop with distance, due to its electrochemical consumption. In case of equimolar biogas (Fig. 2d), H_2 increases faster for high steam content at the inlet (e.g. the line corresponding to $CH_4/CO_2 = 30/30$, steam 40%v), due to the higher extent of CH_4 steam reforming, but after most of the CH_4 is consumed, H_2 concentration declines faster, in these cases, resulting in a situation in which high CO_2 leads to higher H_2 concentrations, after the first centimeter from the cell inlet. Taking into account the behavior of CO_2 and steam concentration in Fig. 2c, this situation can be attributed to the rapid equilibrium of WGS (Reaction 2). Klein et al. [22] examined the kinetics of both Reactions 1 and 2, for CH_4 gradual and direct internal reforming (in the absence of CO_2 feed). The present results suggest that such an analysis (available with data presented herein) would also be interesting in the case of biogas internal reforming. CO, on the other hand, exhibits the same behavior (initial increase according to Reaction 1 and gradual decrease due to Reaction 5), and its concentration, throughout the inlet region is proportional to CO_2 (Fig. 2b) and biogas (Fig. 2d) concentration.

Fig. 3 also depicts the profile of $CH_4/CO_2/H_2O$ (a) and H_2/CO (b) molar fractions with distance x, and for z = 1.70 mm, at the central horizontal axis of the anodic chamber (y = 1.50 mm), at the surface of the anodic electrode (y = 2.50 mm — anode/gas phase interface) and at the anode/electrolyte interface (y = 2.95 mm). In the first centimeter from the inlet, CH_4, steam and CO_2 concentrations (Fig. 3a) are higher in the gas phase of the anode chamber and decrease within the anode electrode ($2.50 < y < 2.95$). In the case of CH_4 and steam, this behavior can be attributed to their consumption through Reaction 1 over the Ni catalyst of the anodic electrode. In the same region ($x < 1$ cm) CO_2 is consumed by the reverse WGS, mostly within the pores of the anodic electrode, where H_2 is catalytically generated. As shown in Fig. 3b, H_2 concentration is higher within the porous anode, due to Reaction 1, and lowers towards the gas phase of the anodic chamber (CO exhibits the same behavior). The situation alters after CH_4 is almost extinct ($x > 1$ cm), where, although the corresponding lines for y = 1.50, 2.50 and 2.95 seem to coincide for all species, CO_2 and H_2O molar fractions appear to be slightly higher near the

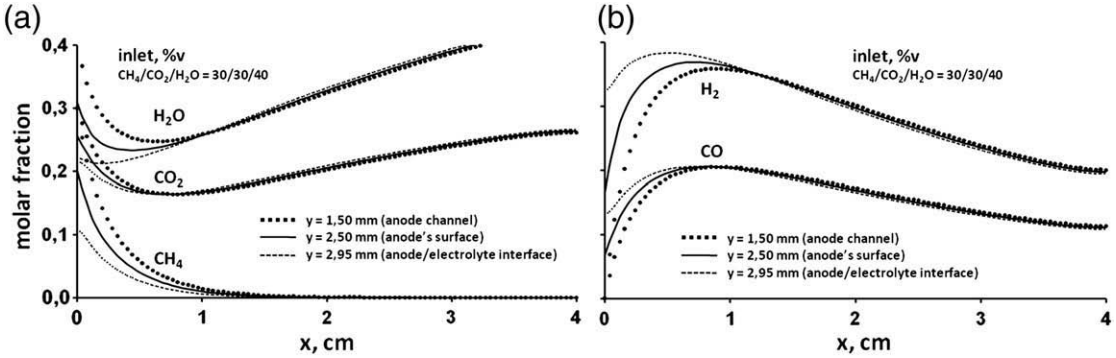

Fig. 3. Comparison of chemical species distribution at y = 1.50 mm (centre of the anode channel), y = 2.50 (anode/gas phase interface) and y = 2.95 (anode/electrolyte interface), for $V_{cell} = 0.5$ V ((a) for reactants and (b) for products).

Please cite this article as: E. Vakouftsi, et al., Solid State Ion. (2010), doi:10.1016/j.ssi.2010.05.051

electrolyte (the opposite stands for H_2 and CO — Fig. 3b) due to the domination of the electro-oxidation reactions, in this region.

3.2. Temperature gradients

Reforming reactions can cause a steep temperature decrease at the inlet of a SOFC, before their endothermicity is counterbalanced by the exothermic H_2/CO electro-oxidation, and result disastrous thermal stresses to the SOFC's ceramic components [30,31]. In this context, Fig. 4a depicts the variation of the temperature of the anodic electrode (at its centre, y = 2.725 mm), the electrolyte (y = 3 mm) and the cathodic electrode (y = 3.225 mm), with the distance x from the unit cell's inlet, and for constant CH_4 molar fraction at the feed. Taking into account that all biogas/steam mixtures were assumed to enter the anodic compartment at 1073 K (the same stands also for the co-flow of air in the cathode), the temperature of the electrolyte and the electrodes is lower at the inlet (x = 0 mm), due to the cooling effect of the endothermic Reaction 1, and gradually increases as CH_4 is consumed and the effect of the exothermic electrochemical oxidations becomes predominant. The endothermic reverse WGS, near the inlet, and the exothermic rightward reaction, beyond the first centimeter, tend to support this behavior. As the endothermic CH_4 steam reforming is conducted catalytically over the anodic Ni phase, the initial temperature is lower at the anodic electrode and increases with y. This results in a temperature difference of approximately 2 K, between the anode and the electrolyte and between the electrolyte and the cathode, at x = 0 mm, which tend to diminish within the first centimeter from the inlet.

On the other hand, the increase of steam supply for constant CH_4 at the inlet (or else the decrease of CO_2 content — Fig. 4a) results in a lower temperature profile throughout the examined inlet region, due to the increased rate of the endothermic Reaction 1. For constant CH_4/CO_2 ratio (equal to unity — Fig. 4b) the increase of the CH_4 content, accompanied by a decrease in steam, leads to higher temperature profiles. This can be attributed to the elevated H_2 and CO concentrations (Fig. 2d) in rich biogas mixtures, supporting higher electro-oxidation rates, and to the decrease in the rate of steam reforming, due to the alleviated steam concentrations.

Fig. 4c and d depicts the temperature gradients within the YSZ solid electrolyte (y = 3 mm), and throughout the examined inlet region (x < 4 cm). For constant CH_4 (Fig. 4c) the maximum temperature gradient appears at about 0.5 cm from the inlet, for all the corresponding biogas/steam mixtures, and its value increases from 10.8 K/cm, in the absence of CO_2 ($CH_4/CO_2/H_2O$ = 30/0/70%v) to 11.6 K/cm, for equimolar biogas ($CH_4/CO_2/H_2O$ = 30/30/40%v). This slight variation is proportional to the temperature decrease at x = 0 mm, which is steeper in the first case due to the enhanced rate of Reaction 1. For equimolar biogas mixtures (Fig. 4d) the variation in maximum values is almost negligible (11.58–11.71 K/cm as biogas/steam ratio increases), but this value shifts away from the inlet (from x = 0.36 to x = 1.09 cm) with the decrease of the steam content. Although this rightward shift matches with the shift of maximum H_2 and CO contents (Fig. 2d), a more thorough explanation based on an analysis of the accurate kinetics of the involved chemical and electrochemical phenomena, should be attempted in a future work.

3.3. Carbon deposition

Carbon formation, due to the side reactions of CH_4 cracking and Boudouard:

$$CH_4 \leftrightarrow C + 2H_2 \quad (7)$$

$$2CO \leftrightarrow C + CO_2 \quad (8)$$

is a serious problem for CH_4 fed SOFCs [6,7]. Following the analysis performed by Klein et al. [22], the present results can lead to an estimation of whether or not carbon deposition is thermodynamically

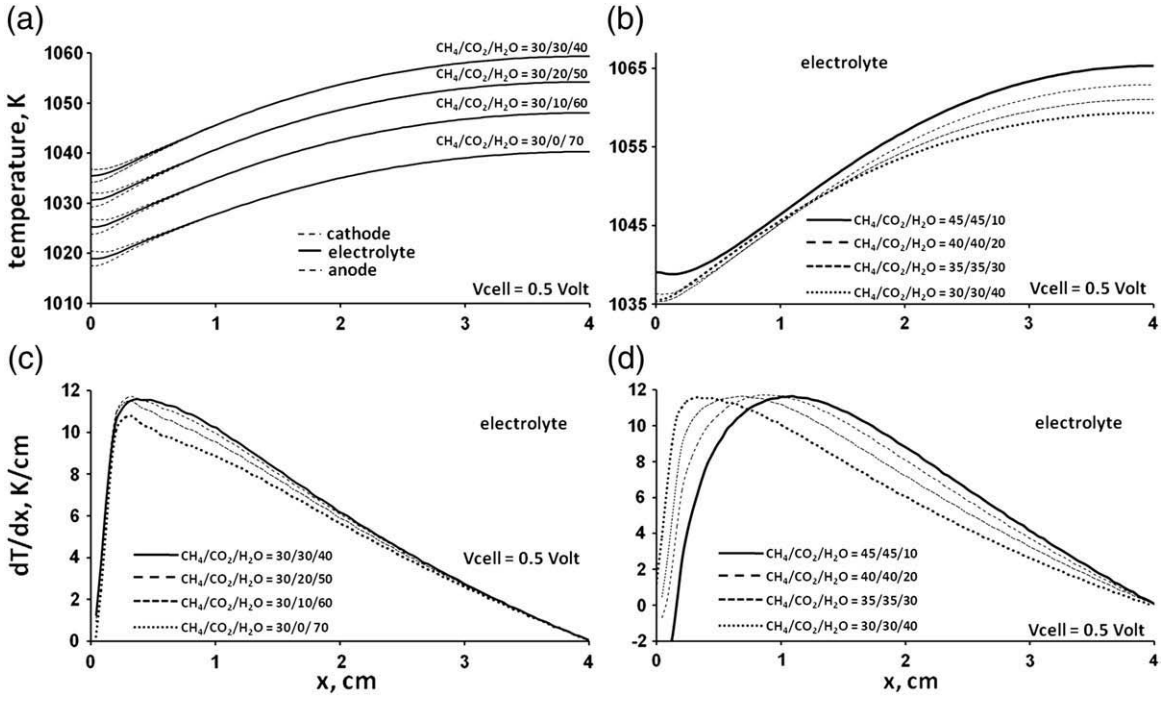

Fig. 4. Temperature ((a) for constant CH_4 inlet and (b) for equimolar CH_4/CO_2 = 1 ratio) and temperature gradient ((c) for constant CH_4 inlet and (d) for equimolar CH_4/CO_2 = 1 ratio) distribution along the unit cell.

Please cite this article as: E. Vakouftsi, et al., Solid State Ion. (2010), doi:10.1016/j.ssi.2010.05.051

favored or prohibited. According to this analysis, the values of α and β parameters, defined as:

$$\alpha = \frac{P_{CO2}\alpha_{carbon}}{P_{CO}^2 K_{boudouard}} \beta = \frac{P_{H2}^2 \alpha_{carbon}}{P_{CH4} K_{cracking}} \quad (9)$$

represent the driving forces for carbon deposition ($\alpha_{carbon}=1$, is the solid carbon activity on the anodic catalytic sites and $K_{boudouard}$/$K_{craking}$ are the corresponding equilibrium constants). In case α or β<1, carbon deposition is thermodynamically favored and the reaction will proceed rightwards, while for α or β>1, carbon formation is thermodynamically impossible (equilibrium stands for α or β=1). The local values of α and β can be calculated from the distributions of temperatures and partial pressures within the porous anode, predicted by the applied CFD model. The simultaneous influences of both reactions can be estimated by coefficient γ=α×β [22], since even in the case that only the cracking reaction yields solid carbon (β<1), an α value sufficiently higher than unity denotes the decoking role of the reverse Boudouard reaction [22]. It must be noted here, that despite the fact that all the examined conditions were chosen so as to prevent carbon deposition, γ values throughout the unit cell can lead to useful remarks.

In this context, Fig. 5a and b depicts the calculated γ values, for the examined biogas/steam mixtures at an imposed $V_{cell}=0.5$ V, and shows that the greater possibility for coke formation stands for CH_4 steam reforming mixture ($CH_4/CO_2/H_2O=30/0/70$), i.e. in the absence of CO_2 at the feed, and at x=0 (depicted values correspond to the anode/gas phase interface — y=2.50 mm). Moreover, the CH_4 steam reforming line ($CH_4/CO_2/H_2O=30/0/70$%v) exhibits a γ profile different to those of combined steam and dry reforming, involving a steep decrease of γ towards x=0 mm, which can be explained by the low CO_2 molar fraction in this region (30/0/70 line in Fig. 2a). Regarding equimolar biogas diluted in steam (dashed lines in Fig. 5a), γ values exhibit a minimum within the first cm from the unit cell's inlet, and despite the fact that all calculated γ values clearly exceed unity, the possibility for carbon deposition is higher at rich methane mixtures. On the other hand, Fig. 5b shows that the partial substitution of steam by CO_2 alleviates this possibility at x=0, and although γ values decrease with CO_2, within the first cm from the inlet, all lines coincide beyond this region. Even for dry biogas feeds (without steam supply at the inlet) in SOFCs, extensive coking is not observed under closed circuit operation, due to the electro-oxidation reactions of carbon, which inhibit its accumulation, as reported by Yentekakis [6,7] and Moon [5].

Fig. 5c examines the profiles of γ values within the porous structure of the anodic electrode (2.50<y<2.95 mm), and shows that the possibility for carbon deposition is greater at the anode/gas phase interface (y=2.50 mm), for both the steam reforming ($CH_4/CO_2/H_2O=30/0/70$%v) and the equimolar biogas ($CH_4/CO_2/H_2O=45/45/10$%v) mixtures. This estimation can be attributed to the decrease of the CH_4's molar fraction, from the anodes surface (y=2.50 mm) to the anode/electrolyte interface (y=2.95 mm), and despite the fact that CO_2 also exhibits the same trend (Fig. 3a). In this context, Fig. 5d shows that β values (the driving force for carbon deposition through CH_4 cracking) are lower than unity (the rightward direction of Reaction 7 is favored by thermodynamics) for both mixtures. But the corresponding values of α are adequately high to prevent carbonization (decoking by the reverse Boudouard), and to lead to the γ values presented in Fig. 5c. Moreover, β values increase with y (from the anode's surface to the anode/electrolyte interface) as the CH_4's molar fraction decreases in the same direction (Fig. 3a), while the α values follow the opposite trend.

3.4. SOFC performance

Finally, Fig. 6a shows that equimolar biogas, or else the substitution of steam by the CO_2 reforming agent for the same CH_4 content in the feed, leads to higher operational voltages, and consequently to higher power densities. Yentekakis et al. [6,7], studied a number of dry (no steam addition at inlet) biogas compositions in high and intermediate temperature SOFCs and reported superior power outputs in the case of equimolar CH_4/CO_2 mixtures. This was related to the fact that the rate of the internal CO_2-reforming of CH_4 is maximized at this composition [6]. Kinetic studies of the CH_4 dry reforming over Ni-YSZ cermets document the competitive adsorption of CH_4 and CO_2 on the Ni surface, leading to a maximum rate for equimolar CH_4/CO_2 mixtures [7]. Maximum rates of

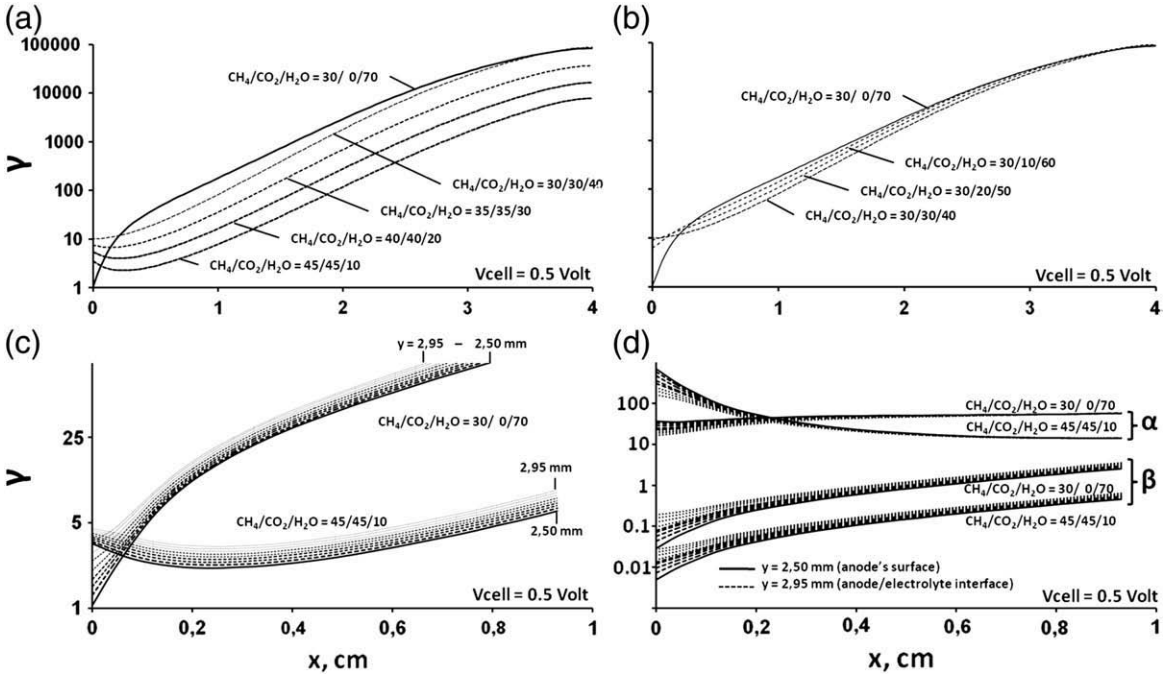

Fig. 5. Estimation of the possibility for carbon deposition along the unit cell.

Please cite this article as: E. Vakouftsi, et al., Solid State Ion. (2010), doi:10.1016/j.ssi.2010.05.051

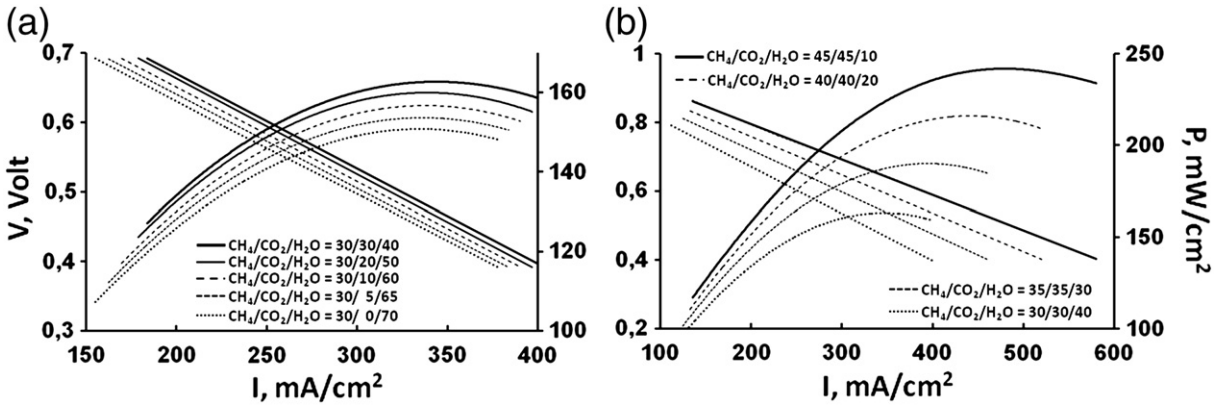

Fig. 6. Current-potential-power curves for the examined biogas/steam mixtures ((a) for constant CH_4 inlet and (b) for equimolar $CH_4/CO_2 = 1$ ratio).

CH_4 consumption result in increased concentrations of H_2 and CO, which are expected to enhance the rates of the corresponding electrochemical steps and consequently the electrical power generation [6]. Fig. 6a also shows that biogas feeds with higher ratio of CH_4 over CO_2 do not cause a significant decrease in cell power output (the increase of CH_4/CO_2 ratio from 30/30 to 30/10 for constant CH_4 input, decrease maximum power density by less than 6%), also in agreement to Yentekakis [7], while the minimization of the steam addition, for equimolar biogas feed (Fig. 6b) improves performance significantly (the decrease of steam addition from 40 to 10%v increases maximum power output by almost 50%).

4. Conclusions

In the present work full-field solutions of the mass, heat and momentum transfer equations were combined to the chemical and electrochemical phenomena within the inlet region of a planar SOFC unit-cell configuration fed with biogas/steam mixtures. Species, temperature and current distribution profiles supported certain estimations of crucial phenomena such as the development of thermal stresses and the possibility of carbon deposition. Regarding thermal gradients, maximum values of 11–12 K/cm, within the first cm from the inlet, were predicted. These values were not significantly affected by the H_2O/CO_2 ratio, and appear to be slightly higher than the commonly accepted safety limit of 10 K/cm [30]. Based on the present results, a more thorough study regarding the dependence of temperature gradients on the volumetric flowrate and the temperature of the feed, as well as the possibility to co-supply minor amounts of gas phase oxygen to the anode, ought to be performed. On the other hand, carbon deposition is not thermodynamically favored under the examined $CH_4/CO_2/H_2O$ ratios and operational conditions, in accordance to the relevant literature. Nevertheless, the performed analysis is based on thermodynamic estimations, and a detailed kinetic study of the involved coking/decoking reactions could provide a more accurate picture. Finally, the current–potential curves of the examined unit cell confirmed that equimolar biogas maximizes power output, although increased CH_4/CO_2 ratios, which decrease the possibility of carbon deposition, only slightly affect performance. On the contrary, steam dilution of biogas results in significant voltage (and power) losses.

Notation

$[A/V]_{eff}$	effective surface to volume ratio of the electrodes
$[C_i]$	near-wall molar concentration of the i species
$[C_{i,ref}]$	molar concentration at a reference state at inlet
d_p	pore diameter
j_0	exchange current density
k_S	thermal conductivity of the solid parts of a porous medium
P_i	partial pressure of specie i
T	temperature
α_a,α_c	anodic and cathodic charge transfer coefficients
α_k	concentration exponent
ε	porosity
η	overpotential
κ	permeability (the square of volume/surface of the porous material)
σ_F,σ_S	ionic and solid phase conductivity, respectively

Acknowledgments

The present research was co-funded by the ESF (75%) and the Hellenic State (25%) through the framework of scientific and technological cooperation between RTD organizations in Greece and in USA, Canada, Australia, New Zealand, Japan, South Korea, Taiwan, Malaysia and Singapore.

References

[1] J. Van herle, F. Marechal, S. Leuenberger, M. Membrez, O. Bucheli, D. Favrat, J. Power Sources 131 (2004) 127–141.
[2] J. Van herle, Y. Membrez, O. Bucheli, J. Power Sources 127 (2004) 300–312.
[3] C.G. Vayenas, S.I. Bebelis, I.V. Yentekakis, S.N. Neophytides, Electrocatalysis and Electrochemical Reactors, in: P.J. Gellings, H.J.M. Bouwmeester (Eds.), The CRC Handbook of Solid State Electrochemistry, CRC Press, 1997, p. 445, (Chapter 13).
[4] S.C. Singhal, K. Kendall, High Temperature Solid Oxide Fuel Cells, Elsevier Ltd., 2003
[5] D.J. Moon, J.W. Ryu, Catal. Today 87 (2003) 255.
[6] I.V. Yentekakis, T. Papadam, G. Goula, Solid State Ionics 179 (2008) 1521.
[7] I.V. Yentekakis, J. Power Sources 160 (2006) 422.
[8] J. Staniforth, K. Kendall, J. Power Sources 86 (2000) 401.
[9] Y. Shiratori, T. Oshima, K. Sasaki, Int. J. Hydrogen En. 33 (2008) 6316.
[10] P. Costamagna, P. Costa, V. Antonucci, Electrochim. Acta 43 (1998) 375.
[11] A. Virkar, J. Chen, C. Tanner, J. Kim, Solid State Ionics 131 (2000) 189.
[12] S. Chan, X. Chen, K. Khor, J. Electrochem. Soc. 151 (1) (2004) A164.
[13] P. Costamagna, K. Honegger, J. Electrochem. Soc. 145 (11) (1998) 3995.
[14] C.O. Colpan, I. Dincer, F. Hamdullahpur, Int. J. Hydrogen En. 32 (2007) 787.
[15] H. Zhu, R.J. Kee, J. Power Sources 161 (2006) 957.
[16] T. Ackmann, L. de Haart, W. Lehnert, D. Stolten, J. Electrochem. Soc. 150 (6) (2003) 783.
[17] P. Li, K. Suzuki, J. Electrochem. Soc. 151 (4) (2004) 548.
[18] H. Yakabe, T. Sakurai, Solid State Ionics 174 (2004) 295.
[19] S. Campanari, P. Iora, J. Power Sources 132 (2004) 113.
[20] D. Sanchez, R. Chacartegui, A. Munoz, T. Sanchez, Int. J. Hydrogen En. 33 (2008) 1834.
[21] P. Piroonlerkgul, N. Laosiripojana, A.A. Adesina, S. Assabumrungrat, Chem. Eng. Process 48 (2009) 672.
[22] J. Klein, Y. Bultel, S. Georges, M. Pons, Chem. Eng. Sci. 62 (2007) 1636.
[23] J. Klein, S. Georges, Y. Bultel, J. Electrochem. Soc. 155 (4) (2008) B333.
[24] J. Klein, Y. Bultel, M. Pons, P. Ozil, J. Appl. Electrochem. 38 (2008) 497.
[25] P.A. Ramakrishna, Shi Yang, C.H. Sohn, J. Power Sources 158 (2006) 378.
[26] J. Klein, Y. Bultel, M. Pons, P. Ozil, J. Fuel Cell Sci. Technol. 7 (2007) 425.
[27] K. Hou, R. Hughes, Chem. Eng. J. 82 (2001) 311.
[28] S. Mazumder, J.V. Cole, J. Electrochem. Soc. 150 (11) (2003) A1503.
[29] E. Vakouftsi, G. Marnellos, C. Athanasiou, F. Coutelieris, Defect Diffus. Forum 87–92 (2008) 273.
[30] L. Lim, D. Chadwick, L. Kershenbaum, Ind. Eng. Chem. Res. 44 (2005) 9609.
[31] C. Lin, T. Chen, Y. Chyou, L. Chiang, J. Power Sources 164 (2007) 238.